Article

Neuron

Coupled Activation of Primary Sensory Neurons Contributes to Chronic Pain

Highlights

- Tissue injury induces DRG neuronal coupling that adjacent neurons activate together
- The coupled activation is mediated by an injury-induced upregulation of gap junctions
- DRG neuronal coupling contributes to pain hypersensitivity
- Inhibiting gap-junction-mediated coupling may provide a way to relieve chronic pain

Authors

Yu Shin Kim, Michael Anderson, Kyoungsook Park, ..., Yun Guan, David C. Spray, Xinzhong Dong

Correspondence

yukim@utmb.edu (Y.S.K.), xdong2@jhmi.edu (X.D.)

In Brief

Using in vivo DRG imaging, Kim et al. discovered a neuronal coupling phenomenon that adjacent neurons tend to activate together following tissue injury. This coupled activation, mediated by an upregulation of gap junctions in the DRG, contributes to pain hypersensitivity.

Kim et al., 2016, Neuron *91*, 1085–1096
September 7, 2016
http://dx.doi.org/10.1016/j.neuron.2016.07.044

CellPress

Neuron
Article

Coupled Activation of Primary Sensory Neurons Contributes to Chronic Pain

Yu Shin Kim,[1,2,9,*] Michael Anderson,[1,9] Kyoungsook Park,[1,9] Qin Zheng,[1,9] Amit Agarwal,[1] Catherine Gong,[1] Saijilafu,[3,4] LeAnne Young,[1] Shaoqiu He,[6] Pamela Colleen LaVinka,[1] Fengquan Zhou,[3] Dwight Bergles,[1] Menachem Hanani,[5] Yun Guan,[6] David C. Spray,[7] and Xinzhong Dong[1,8,*]

[1]Departments of Neuroscience, Neurosurgery, and Dermatology, Center of Sensory Biology, the Johns Hopkins University School of Medicine, 725 N. Wolfe Street, Baltimore, MD 21205, USA
[2]Department of Neuroscience & Cell Biology, the University of Texas Medical Branch School of Medicine, 301 University Boulevard, Galveston, TX 77555, USA
[3]Department of Orthopaedic Surgery, the Johns Hopkins University School of Medicine, 725 N. Wolfe Street, Baltimore, MD 21205, USA
[4]Department of Orthopaedics, the First Affiliated Hospital, Orthopaedic Institute, Soochow University, People's Republic of China
[5]Hadassah-Hebrew University Medical Center, Mt. Scopus, Jerusalem 91240, Israel
[6]Department of Anesthesiology, the Johns Hopkins University School of Medicine, 725 N. Wolfe Street, Baltimore, MD 21205, USA
[7]The Dominick P. Purpura Department of Neuroscience, Albert Einstein College of Medicine, Bronx, NY 10461, USA
[8]Howard Hughes Medical Institute, the Johns Hopkins University School of Medicine, Baltimore, MD 21205, USA
[9]Co-first author
*Correspondence: yukim@utmb.edu (Y.S.K.), xdong2@jhmi.edu (X.D.)
http://dx.doi.org/10.1016/j.neuron.2016.07.044

SUMMARY

Primary sensory neurons in the DRG play an essential role in initiating pain by detecting painful stimuli in the periphery. Tissue injury can sensitize DRG neurons, causing heightened pain sensitivity, often leading to chronic pain. Despite the functional importance, how DRG neurons function at a population level is unclear due to the lack of suitable tools. Here we developed an imaging technique that allowed us to simultaneously monitor the activities of >1,600 neurons/DRG in live mice and discovered a striking neuronal coupling phenomenon that adjacent neurons tend to activate together following tissue injury. This coupled activation occurs among various neurons and is mediated by an injury-induced upregulation of gap junctions in glial cells surrounding DRG neurons. Blocking gap junctions attenuated neuronal coupling and mechanical hyperalgesia. Therefore, neuronal coupling represents a new form of neuronal plasticity in the DRG and contributes to pain hypersensitivity by "hijacking" neighboring neurons through gap junctions.

INTRODUCTION

Dorsal root ganglion (DRG) are aggregates of the somata of 10,000–15,000 primary sensory neurons (Schmalbruch, 1987; Sørensen et al., 2003), which play an essential role in initiating somatosensation by detecting sensory stimuli in the periphery and sending signals to the spinal cord via their axons (Basbaum et al., 2009). DRG neurons are highly diverse in terms of cell sizes, gene expression, myelination levels, etc. While small-diameter neurons are the pain-sensing neurons, medium- to large-diameter neurons preferentially detect low-threshold, non-painful mechanical stimulation (Basbaum and Woolf, 1999; Liu and Ma, 2011). Pathological conditions, such as inflammation and nerve injury, can sensitize DRG neurons, causing heightened pain sensitivity, often leading to chronic pain. In addition, each DRG neuronal soma is surrounded by multiple satellite glial cells (SGCs) (Hanani, 2005; Pannese, 2010). There is evidence for intercellular communications within sensory ganglia, involving both neurons and SGCs (Hanani, 2012; Huang et al., 2013). This communication can be altered by injury. Although the mechanisms of hypersensitivity of individual neurons have been extensively studied, how DRG neurons function at a population level as an ensemble under physiological and pathological conditions is unclear due to the lack of suitable tools.

In this report, we developed an imaging technique that allowed us to simultaneously monitor the activation of >1,600 neurons/DRG in response to sensory stimulation applied to the skin in live mice. Using this powerful technique, we discovered a striking neuronal coupling phenomenon that adjacent neurons tend to activate together following inflammation or nerve injury, although this rarely happens in naive animals. This coupled activation occurs among various sizes of neurons, including small-diameter nociceptors and large-diameter low-threshold mechanoreceptors (LTMRs). The transfer of membrane-impermeable dye between coupled activating neurons suggests that the coupled activation is likely due to direct cell-to-cell communication. Combining the imaging technique with pharmacological and genetic approaches, we found that the coupling is mediated by an injury-induced upregulation of gap junctions in SGCs surrounding DRG neurons. Blocking gap junctions significantly attenuated neuronal coupling in the DRG and also reduced mechanical hyperalgesia. Therefore, neuronal coupling represents a new form of neuronal plasticity in the DRG, and by

"hijacking" neighboring neurons through gap junctions, it contributes to pain hypersensitivity.

RESULTS

Development of In Vivo DRG Imaging Technique

In order to monitor the activity of large populations of DRG neurons in intact live animals, we developed an in vivo imaging technique using *Pirt-GCaMP3* mice, in which the genetic-encoded Ca^{2+} indicator GCaMP3 is specifically expressed in >95% of all DRG neurons under the control of the *Pirt* promoter (Kim et al., 2014). For the in vivo imaging from anesthetized *Pirt-GCaMP3* mouse, we first surgically exposed the dorsal aspect of the right lumbar 4 (L4) DRG, which innervates the right hindpaw, leg, thigh, and back of the mouse. Then the animal was laid on its abdomen on the stage under a Leica LSI confocal microscope with a long-working distance lens (Figure 1A). The spinal column was clamped to minimize movements from breathing and heart beats. During the imaging session, which usually lasted 3–4 hr, the animal was under constant isoflurane anesthesia, and its body temperature was kept at 37°C with a heat pad. Because the surface of DRG is curved, z stack imaging is required to cover the entire area of exposed L4 DRG. Strikingly, an average of 1,607 ± 27 neurons per DRG (~15% of total DRG neurons) could be imaged at ~6.35 s/frame (Figures 1B and 2A). To determine how well the imaged neurons represent the whole population of the ganglion, we injected the neuronal tracer 1,1′-dioctadecyl-3,3,3′,3′-tetramethylindocarbocyanine perchlorate (DiI) into the hindpaws and found that the DiI-labeled somata were evenly distributed in the DRG (Figures 1C and 1D). These data suggest that somata that send axons to the hindpaw are not clustered in a particular region of the DRG and the 1,600 neurons imaged are representative of the entire neuronal population. To determine the extent of DRG neurons responding to sensory stimuli in the receptive field, we performed hindpaw DiI retrograde tracing combined with GCaMP imaging experiments using naive *Pirt-GCaMP3* mice (Figures 1E and 1F). We stimulated the hindpaw with either mechanical force (see details in the next section) or chemicals. We found that 26.4% and 27.6% of DiI-labeled neurons responded to the press of the hindpaws and the capsaicin injection into the hindpaw, respectively, and 3.4% of DiI-labeled neurons responded to both stimuli. The rest of DiI-labeled neurons did not respond to either stimulus. These data indicate that GCaMP3 imaging under isoflurane anesthesia allowed us to image a large portion (>50%) of neurons that innervate the receptive field. Furthermore, using a different anesthesia (i.e., pentobarbital), a similar number of neurons are activated by the same pressure (Figure 1I).

To test the specificity of neuronal activation monitored by GCaMP3 in vivo imaging, we generated *Pirt-GCaMP3;TRPV1*$^{-/-}$ mice and *Pirt-GCaMP3;TRPA1*$^{-/-}$ mice (Figures 1G and 1H). As expected, the injection of capsaicin or mustard oil into the hindpaws evoked robust neuronal activation in the L4 DRG of *Pirt-GCaMP3* wild-type (WT) mice, whereas few GCaMP3 signals were detected in *Pirt-GCaMP3;TRPV1*$^{-/-}$ mice or *Pirt-GCaMP3;TRPA1*$^{-/-}$ mice, respectively. These data suggest that GCaMP signals detected during in vivo DRG imaging are ligand/channel specific.

Increased Activation of Small-Diameter Neurons Contributes to Mechanical Hyperalgesia

For mechanical-force-evoked intracellular Ca^{2+} transient in neurons, we used a rodent pincher analgesia meter instead of von Frey filaments, which allowed us to accurately apply and monitor mechanical force to a large area of the hindpaws. We first determined the force needed to evoke pain responses using the device. Because of the large contact surface area of the pincher, the paw withdrawal threshold (PWT) in naive mice is close to 500 g (Figure 2B), which is much higher than the force normally applied with the thinner von Frey filaments; however, the pressure is similar. The PWTs were substantially lower (~250 g) in mice with inflammation in the hindpaw caused by complete Freund Adjuvant (CFA) injection or chronic constriction injury (CCI) of sciatic nerves (SNs) (Figure 2B). Therefore, mechanical hyperalgesia and allodynia under inflammatory and nerve injury conditions were reliably evoked and accurately measured by the device. To activate neurons during the imaging experiments, we applied 250–300 g force onto the hindpaw, a force that was not enough to induce a paw withdrawal response in naive mice but well above the PWT after injury. The basal GCaMP3 green fluorescence level was low in the DRG (Figures 2C and 2E, left panels). Hindpaw stimulation evoked robust and transient Ca^{2+} increases in a few neurons in naive mice, on average 12.7 ± 3.0 per DRG (Figures 2C and 2E, right panels, and Figures 2D and 2F; Movie S1). However, the number of activated neurons was more than doubled to 42.8 ± 4.5 and 32.3 ± 6.3 in the DRGs of CFA- and CCI-treated mice, respectively (Figure 2G; Movie S2). The average Ca^{2+} transients in activated neurons from injured animals were significantly higher than those from naive animals (Figures 2D and 2F). The diameters of the somata of activated neurons in the injured animals were significantly smaller than those in naive mice (23.0 ± 1.2 μm for control versus 20.2 ± 0.4 μm for CFA and 19.9 ± 0.4 μm for CCI) (Figure 4A). The proportion of the neurons activated by pressure that were in the small-diameter (20 μm) category was also significantly higher in CFA-treated mice compared with controls (52.5% ± 4.4% for CFA versus 28.9% ± 2.6% for control; Figure 2H). These data correlate well with the results from behavioral tests, suggesting that the increased activation of small-diameter neurons (presumably nociceptors) contributes to mechanical hyperalgesia.

Neuronal Coupling Occurs after Tissue Injury

We noticed a striking pattern of neuronal activation in the DRG of injured mice: many activated neurons (13.1 ± 1.7 and 9.8 ± 2.6 neurons/imaged DRG for CFA and CCI, respectively) were adjacent to each other and formed clusters of two to five cells, a phenomenon we called "coupled activation" (Figures 3A and 3B; Movie S3). Neuronal coupling was defined as two or more neuronal cell bodies located within 1 μm of each other showing increases in GCaMP signals between two imaging frames (0.47 s/frame; see faster scanning below). Importantly, coupled activation was rarely seen in naive animals (1.3 ± 0.5 neurons/DRG). In CFA-injected mice, 29.0% ± 1.8% of total activated neurons were coupled activated compared with 5.0% ± 1.7% in DRG from naive mice (Figure 3C). Similar results were obtained for the CCI mice (29.2% ± 8.4% of total activated neurons versus 6.4% ± 1.6% for sham-operated mice). In addition,

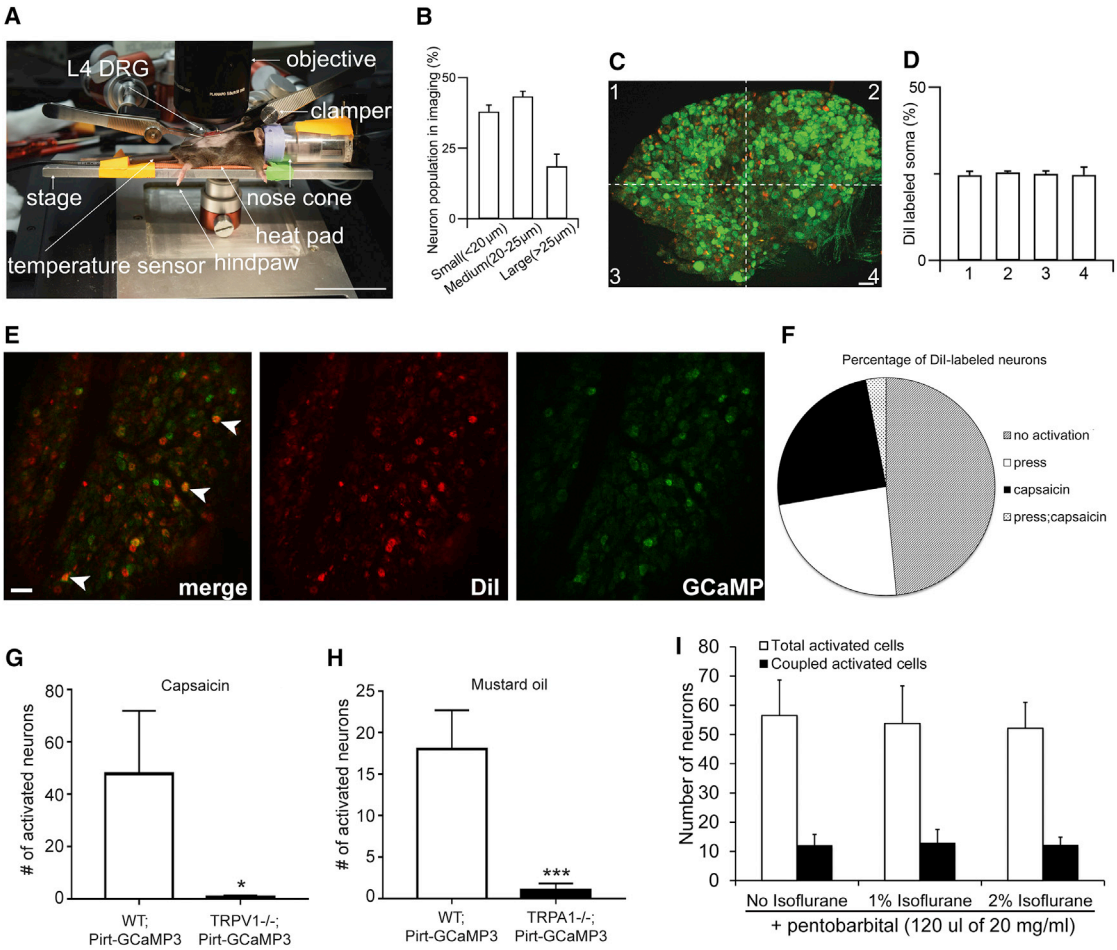

Figure 1. Development of In Vivo DRG Imaging Technique

(A) Imaging stage and animal position of in vivo intact whole L4 DRG under the microscope. After in vivo DRG surgery, the skin is retracted to expose the DRG, and the animal rests on a stage attached to two spinal vertebrae clampers on the rostral (L3) and caudal (S1) area. L4 DRG on the right side is exposed, and the surface of the DRG is imaged through 5× 0.5 NA macro dry objective using Leica LSI confocal microscope with 488 green and 568 red diode lasers. 1% to 2% gas isoflurane is delivered to an animal through a nose cone. A temperature sensor is sensing the animal's rectal body temperature, and its body temperature is controlled by a heat pad on the stage. Sensory stimulation (mild mechanical press) is applied to hindpaw.

(B) Size distribution of small, medium, and large neurons in in vivo calcium imaging of whole L4 DRG of primary sensory neurons. Quantification of cell sizes was performed after imaging of whole L4 DRG neurons from *Pirt-GCaMP3* mice (n = 12).

(C) Distribution of hindpaw-projected neurons at L4 DRG level. A hindpaw of *Pirt-GCaMP3* mice was DiI injected and imaged several days later (A). Green signal is GCaMP3 protein and red color is DiI-labeled DRG neurons in L4 DRG (n = 7). Scale bars, 40 μm.

(D) Hindpaw-projected neurons are evenly located and distributed on the L4 DRG ganglia.

(E) Determine the proportion of hindpaw-innervating neurons being activated by stimuli applied to the receptive field. A hindpaw of naive *Pirt-GCaMP3* mice was DiI (10 μL of 1 mg/mL, subcutaneously, s.c. plantar surface) injected and imaged 7 days later. GCaMP3 signals were evoked by either pressing the hindpaw (300 g) or capsaicin injection (10 μL of 3.3 mM in 0.9% saline, s.c. plantar surface) into the hindpaw (data not shown). Arrowheads indicate DiI-labeled neurons being activated by pressing the hindpaw. Scale bars, 40 μm.

(F) Percentage of DiI-labeled neurons activated by press (26.4%), capsaicin injection (27.6%), or both (3.4%). n = 3.

(G and H) Activation of L4 DRG neurons in response to capsaicin (G; 10 μL of 3.3 mM) or mustard oil (H; 10 μL of 40 mM) was determined by in vivo DRG imaging using Pirt-GCaMP3 in wild-type (WT; Pirt-GCaMP3; n = 4) or Pirt-GCaMP3 in TRPV1 knockout (TRPV1$^{-/-}$;Pirt-GCaMP3; n = 3) or TRPA1 knockout (TRPA1$^{-/-}$;Pirt-GCaMP3; n = 4) mice. *p < 0.05, ***p < 0.005. Unpaired Student's t test.

(I) Determine the effects of different anesthetic reagents on DRG imaging. CFA-treated Pirt-GCaMP3 mice were imaged in the presence of pentobarbital (120 μL of 20 mg/mL, i.p.) with no, 1%, or 2% of isoflurane (n = 4). L4 DRG neurons were activated by 300 g press on the hindpaws. The data are presented as mean ± SEM.

we performed in vivo DRG imaging 7 days after CFA injection as the animal is recovering from peak inflammation and found that 12.9% ± 0.7% of total activated neurons are coupled, which is significantly lower than that of 2 days post-CFA (29.0%).

We then imaged the entire DRG to identify coupled activated neurons and verified coupling events using a much higher scanning speed by zooming in on one ensemble of neurons. For this experiment, we used *Pirt-GCaMP6* mice, which we recently

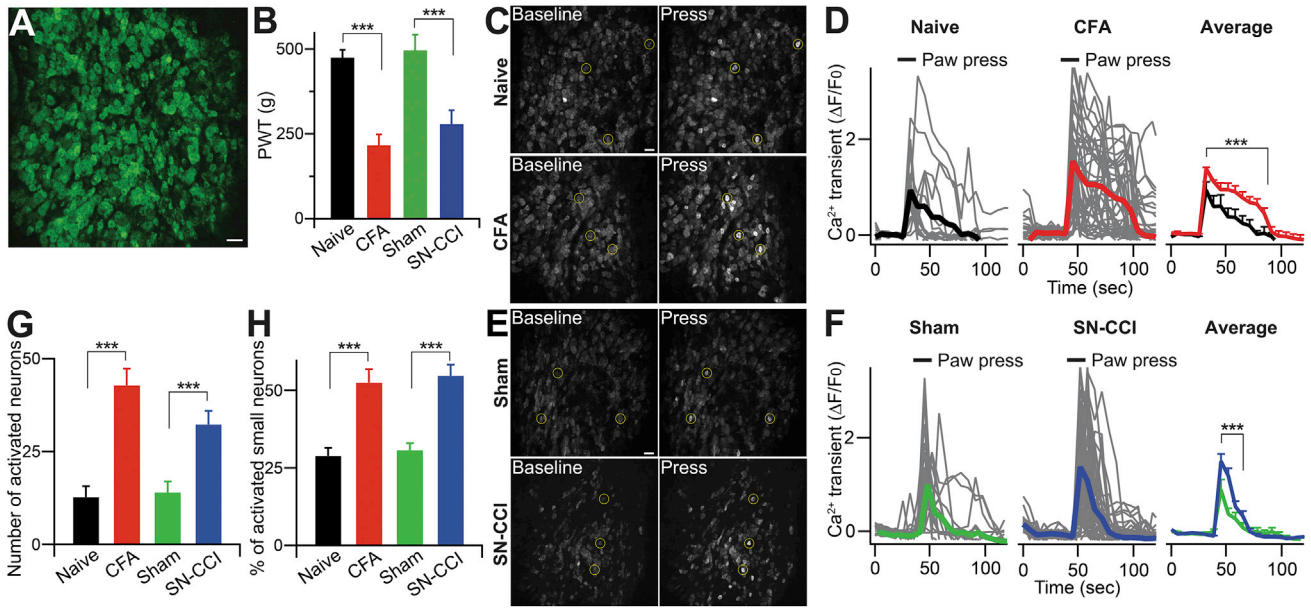

Figure 2. In Vivo Calcium Imaging in Whole L4 DRG of Primary Sensory Neurons

(A) Representative in vivo DRG calcium imaging using *Pirt-GCaMP3*. In vivo whole L4 DRG neurons were activated by 100 mM KCl. Scale bar, 50 μm.

(B) Paw withdrawal threshold (PWT) was tested at the hindpaw of naive, CFA, sham, and SN-CCI animals with rodent pincher analgesia meter. The data are expressed as a PWT value and presented as mean ± SEM. CFA, complete Freund's Adjuvant; SN-CCI, sciatic nerve chronic constriction injury.

(C–F) Representative in vivo DRG calcium images showing $[Ca^{2+}]_{in}$ increase in DRG neurons (C and E). Time course of the amplitude of the calcium transient that was evoked by mild mechanical press (using rodent pincher, 300 g) at the hindpaw from naive, CFA, sham, and SN-CCI animals (D and F). Some examples of activated DRG neurons are circled. Each trace is a response from a single DRG neuron. All data for calcium transient are expressed as the percentage of baseline calcium transient ($\Delta F/F_0$) and are presented as mean ± SEM. Black bars indicate when stimuli were applied. Scale bar, 50 μm.

(G) Number of neurons activated by mild mechanical press to naive, CFA, sham, and SN-CCI animals.

(H) Percentage change of small-diameter neurons (<20 μm) activated by mild mechanical press to naive, CFA, sham, and SN-CCI animals. The data are presented as mean ± SEM. ***$p < 0.001$.

generated by crossing *Pirt-Cre* and *Rosa26-loxP-STOP-loxP-GCaMP6s* mice. Indeed, even with much faster imaging speed (0.47 s/frame), we could still detect the simultaneous activation in the majority of the coupled neurons (9 out of 12 neurons exhibiting simultaneous activation; Figure 4D).

In addition to investigating a single mechanical-force (i.e., ~250 g)-evoked response, we performed the full-dose response of pressure (from very mild 50 g to noxious 500 g) using *Pirt-GCaMP6* mice (Figures 4E–4G). From mild pressure (150 g and 200 g) to noxious pressure (500 g), there are significantly more neurons being activated in naive mice. However, neither the number of coupled activated neurons nor the percentage of coupled neurons over total activated neurons in naive mice are significantly increased between innocuous and noxious pressure. Strikingly, in the CFA-treated mice, both the total number of coupled activated neurons and the percentage of coupled neurons over total activated neurons are significantly increased from mild pressure to noxious pressure and significantly higher than those of naive mice. Together, these data suggest that neuronal coupling is caused by tissue injury.

Although the majority of the coupled activation (75%) occurred simultaneously (i.e., no delayed activation in the coupled neurons at 0.47 s/frame rate) and many different diameter neurons were involved in coupling events (Figures 3D, 4B, and 4C), there were a few coupling events where neurons had delayed longer than 1 s after the first event. The delayed coupled activations were useful for determining which type of following neurons were recruited by which type of leading neurons after injury. To determine whether large-diameter LTMRs participate in coupling activation, we generated *NPY2r-tdTomato;Pirt-GCaMP3*/+ mice. A previous study has shown that NPY-2r is specifically expressed in rapidly adapting Aβ-LTMRs having medium to large diameters (20–30 μm) (Li et al., 2011). We found that some of coupled activating neurons displayed red fluorescent in *NPY2r-tdTomato;Pirt-GCaMP3*/+ mice treated with CFA, indicating that rapid-adapting Aβ-LMTRs are involved (Figure 3E). In addition, we used capsaicin to probe TRPV1-expressing neurons and found that 12.9% of capsaicin-sensitive neurons are coupled activated neurons. Besides studying mechanical-force-evoked neuronal coupling, we performed in vivo DRG imaging in response to noxious heat stimuli using CFA-treated *Pirt-GCaMP3* mice (Figures 4H and 4I). With hindpaw immersion into 48°C water bath, a total of 110 neurons are activated, 14% of which are coupled activated neurons. Interestingly, this 14% coupling rate evoked by noxious heat is significantly lower than that induced by mechanical stimuli (>25%).

Gap Junctions Likely Connect Coupled Activated Neurons

Since DRG from both CCI- and CFA-treated mice displayed similar degrees of coupled activation, we focused on the

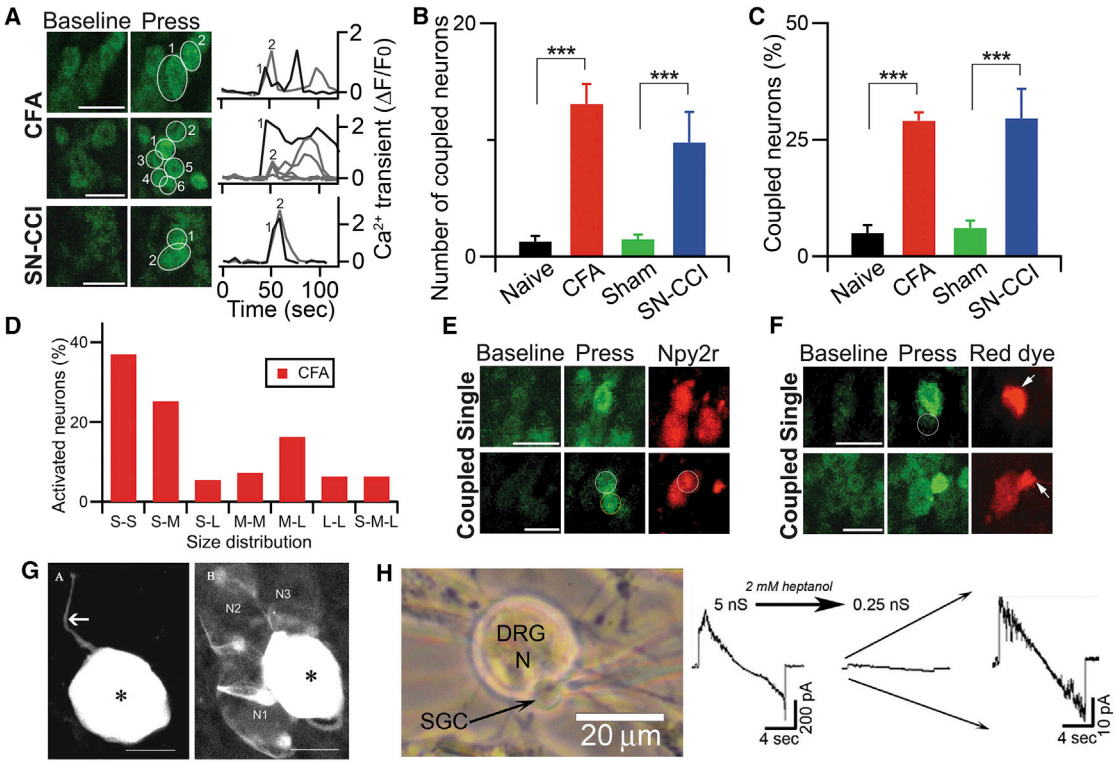

Figure 3. Coupled Activation of Adjacent DRG Neurons in In Vivo DRG Calcium Imaging

(A) Representative images of coupled events in in vivo calcium imaging of whole L4 DRG neurons. Left panels: adjacent DRG neurons tend to activate together when stimuli (mild mechanical press; 300 g) were applied to the hindpaws of CFA and SN-CCI animals. Right panels: time course of the amplitude of the calcium transient that was evoked by mild press at the hindpaw from CFA and SN-CCI animals. Each trace is a response from a single DRG neuron, and number indicates the order of DRG neuron activated by press stimuli. All data for calcium transient are expressed as the percentage of baseline calcium transient ($\Delta F/F_0$). Scale bar, 50 μm.

(B) Number of coupled neurons activated by mild press to naive, CFA, sham, and SN-CCI animals.

(C) Quantification of coupled neurons normalized by total number of neurons activated by mild press to naive, CFA, sham, and SN-CCI animals. ***$p < 0.001$.

(D) Percentage of coupled neurons according to the size of each member of the pair. S, small-diameter DRG neurons (<20 μm); M, medium (20–25 μm); L, large (>25 μm).

(E) Representative in vivo images of neurons labeled for NPY2r-tdTomato, a marker for large-diameter, rapid-adapting low-threshold mechanoreceptor (Aβ-LTMR), and activated singly in naive and coupled in CFA animals. Scale bar, 50 μm.

(F) Representative in vivo images of neurons labeled with rhodamine. Dye transfer was observed only in CFA animals. Circle indicates an adjacent DRG neuron. Arrows indicate where rhodamine was injected into a DRG neuron. Scale bar, 50 μm.

(G) Direct evidence for neuron-SGC coupling by gap junctions. Confocal images obtained with the dye transfer method using intracellular injection of lucifer yellow (LY). Left: an uncoupled neuron with its axon (arrow) in a ganglion from a 3-month-old mouse. Right: a dye-injected neuron (asterisk) was coupled to SGCs around three neighboring neurons (N1–N3) in a ganglion from a 12-month-old mouse. SGCs around the labeled neuron are probably labeled, but they cannot be visualized because of masking by the bright staining of the neuron. Asterisks mark the dye-injected cells. Scale bars, 20 μm.

(H) Dual patch-clamp recordings from neuron-SGC pairs. The cells were clamped at 0 mV, a voltage ramp (from −100 to +100 mV) was applied to the neuron, and current was recorded in an adjacent SGC. Left panel: the configuration of neuron and SGCs is shown. Right panel: the addition of the gap junction blocker heptanol (2 mM) reduced gap-junction-mediated electrical conductance between the neuron and SGC, which was high (5 nS) in the control but was reduced to 0.25 nS by a factor of 20. Scale bar, 20 μm.

simpler CFA model for the subsequent studies. Previous studies have demonstrated that injury induces an increase in dye transfer among glia and between neurons in the DRG, implying the formation of gap junctions in the DRG after injury (Blum et al., 2014; Dublin and Hanani, 2007; Huang et al., 2010). However, how gap junctions influence neuronal activation is unclear. To test the hypothesis that gap junctions are involved in the coupled activation, we injected rhodamine, a low molecular weight red dye that crosses gap junctions, into one of the coupled activated neurons. Strikingly, the red fluorescence appeared in the adjacent co-activated neurons within a few minutes after the injection (Figure 3F). The dye transfer occurred in 4.4% of injected coupled activated neurons, whereas we have never seen any dye transfer from singly activated neurons. These data strongly suggest that coupled activation is mediated by cell-to-cell communication, and gap junctions are good candidates. The 4.4% rate of dye transfer is consistent with the reported low incidence of neuron-neuron dye-coupling after CFA injection in the mouse paw and also in rats after sciatic nerve ligation (Dublin and Hanani, 2007; Zuriel and Devor, 2001).

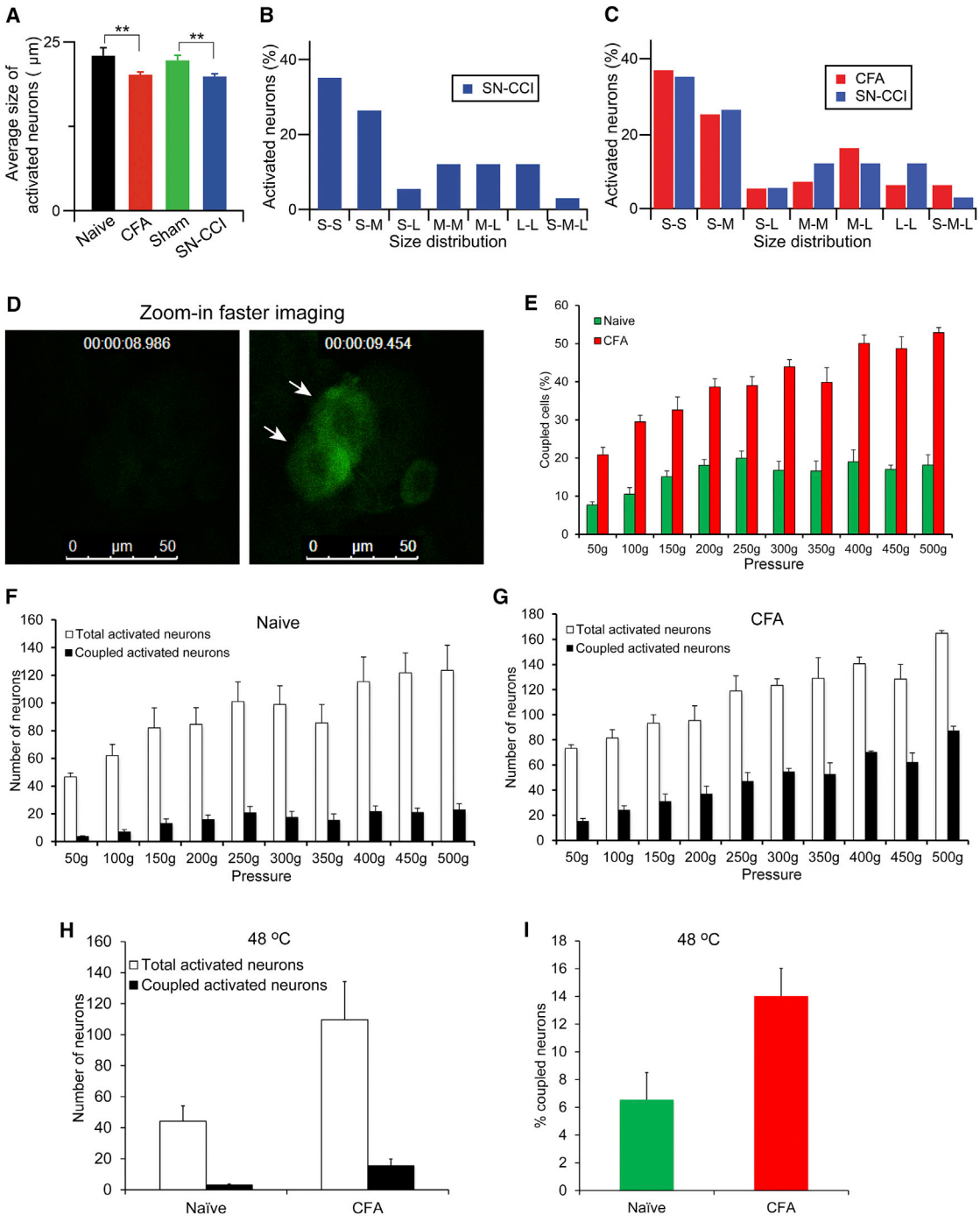

Figure 4. Characterization of Coupled Activated Neurons in the DRG

(A) Average size of activated neurons in in vivo DRG calcium imaging from *Pirt-GCaMP3* mice. Total average size of activated neurons was measured with mild mechanical press stimuli from different conditions (naive, CFA, sham, and SN-CCI) of Pirt-GCaMP3 mice (n = 10).

(B and C) Size distribution of coupled activated neurons. (B) for SN-CCI and (C) for CFA and SN-CCI. Percentage and distribution of coupled activation DRG neurons are determined according to the cell size of each member of the pair. S, small-diameter DRG neurons (<20 um); M, medium (20–25 um); L, large (>25 um).

(D) Examining simultaneous activation by zoomed-in faster imaging. L4 DRG in CFA-treated *Pirt-GCaMP6* mice (n = 3) were imaged first at ~6 s/frame to identify coupled activated neurons in the entire exposed DRG areas. Then imaging was zoomed in on one ensemble of coupled activated neurons with much higher frequency (0.47 s/frame; time point was indicated at the top of the images). Two arrows indicate two simultaneously activated neurons.

(legend continued on next page)

Since SGCs are extremely small and tightly ensheathe neurons, it is impossible to observe them with our imaging system. Instead, we performed glia-neuron dye injection experiment on cultured DRG. SGCs have clear morphological differences and can be easily distinguished from Schwann cell-like glia (see details in our previous study: Belzer et al., 2010). In fact, the vast majority of glia in DRG cultures are SGCs. Indeed, we found that 10% of injected glia exhibited dye transfer to neighboring neurons (Figure 3G). Based on subsequent pharmacological and genetic data, we conclude that monitoring dye transfer is not a sensitive way to determine gap junctions between neurons (directly or indirectly through SGCs). A more sensitive method to detect cell coupling is by patch-clamp recordings from neuron-SGC pairs in dissociated DRG. Recording SGC-neuron pairs showed that 7 of 14 pairs were coupled (with junctional conductances of 8.8 ± 2.6 nS). In all three pairs tested, 2 mM heptanol (a gap junction blocker) uncoupled cells, consistent with gap-junction-mediated coupling (Figure 3H). Similar results were obtained from recording SGC-neuron pairs of acutely dissociated DRG from CFA-treated mice with junctional conductances of 5.6 ± 2.4 nS (7 of 12 pairs; Figure S1). Furthermore, dual patch recordings of neuron-neuron pairs in acutely dissociated DRG from CFA-treated mice showed that electrical coupling occurred in 8 of 18 pairs with the junctional conductance of 0.16 ± 0.07 nS. The junctional conductance suggests that neuron-neuron coupling is weaker than neuron-SGC coupling. Thus, it is conceivable that the observed neuronal coupling is due to neuron-SGC-neuron coupling (see Discussion below).

Blockade of Gap Junctions Reduces Neuronal Coupling and Mechanical Hyperalgesia

We next examined whether the gap junction blocker carbenoxolone (CBX) (Zhang et al., 2009) can inhibit coupled activation. After the first imaging session, which showed that 31.9% ± 3.0% of total activated neurons in CFA-treated mice are activated in clusters, we applied CBX systemically into the mice by intraperitoneal (i.p.) injection (100 mg/kg) (Figures 5A–5C). We performed the second imaging session 1 hr later and found that only 12.5% ± 3.0% of total activated neurons were coupled activated (Figures 5A–5C and comparing Movie S4 for after CBX treatment with Movie S3 for before CBX treatment, respectively). As a control, we injected vehicle in CFA-treated animals and found that it did not significantly reduce the percentage of coupled activation (before 33.5% ± 4.2% versus after 29.1% ± 5.6%; p = 0.51; Figure 5C). This result rules out the possibility that the decreased coupling seen in CBX treatment is due to the desensitization from the multiple imaging sessions and mechanical stimulations. Systemic treatment with heptanol, a different gap junction blocker, also significantly blocked neuronal coupling in CFA-treated mice (25.4% ± 3.8% versus 10.8% ± 2.7% of total activated neurons are coupled for pre- and post [30 min]-injection of heptanol [0.1 mg/kg in 0.9% saline; i.p.; n = 3 per group; p = 0.01]). To minimize indirect actions of CBX, we injected it locally near the coupled activated neurons in the DRG. The results obtained with this local treatment were similar to those observed with systemic CBX (Figures 5D and 5E; Movies S5 and S6). Finally, CBX-treated mice exhibited less mechanical hyperalgesia in CFA and CCI pain models than control vehicle-treated mice (Figure 5F).

Several subtypes of connexin (Cx) proteins, the components of gap junctions, including Cx37, Cx43, and Cx46 have been implicated in chronic pain by previous studies (Garrett and Durham, 2008; Ohara et al., 2008). We were able to detect only Cx43 staining in the DRG, which was restricted to SGCs. The level of Cx43 protein significantly increased in the DRG after injury, but not in the spinal cord (Figures 6A–6D; Figure S2). To directly test whether Cx43 is required for coupled activation, we generated a DRG-specific deletion of Cx43 mice (*PLP-CreER;Cx43*$^{fl/fl}$) from crossing *Cx43*$^{fl/fl}$ mice with *proteolipid protein (PLP)-CreER* mice, which is present in glial cells in the peripheral nervous system such as SGCs (Doerflinger et al., 2003). Anti-Cx43 antibody staining demonstrated that *PLP*-driven *CreER* specifically deleted Cx43 expression in SGCs in the DRG (Figures S2A and S2B), but it was still present in the spinal cord (likely in astrocytes) (Figures S2C and S2D). Therefore, *PLP-CreER;Cx43*$^{fl/fl}$ mice (*Cx43CKO*) allowed us to examine the function of Cx43 in SGCs. In vivo DRG imaging of *PLP-CreER;Cx43*$^{fl/fl}$*;Pirt-GCaMP3*/+ and control littermates, which do not express Cre, showed that deletion of Cx43 in the DRG significantly attenuated the incidence of coupled activation after CFA treatment compared with littermate controls (Figures 6E and 6F). Consistent with this, *PLP-CreER;Cx43*$^{fl/fl}$ mice exhibited less mechanical hyperalgesia than littermates following CFA injection (Figure 6G). However, the mutant mice have normal baseline pain sensitivity as well as normal thermal hyperalgesia after CFA treatment (Figure S1; see Discussion below).

DISCUSSION

Pain manifests itself in a wide range of disorders that debilitate billions of people worldwide, causing heavy societal and health burdens. It is known that DRG neurons are responsible for the detection of noxious stimuli, and their plasticity contributes to persistent pain. However, how DRG neurons function under physiological and pathological conditions are poorly understood due to the lack of suitable tools. Because DRGs are deeply embedded in the vertebrae, it is difficult to record neuronal activity electrophysiologically in situ. Most of the available information is from studies on cultured or isolated ganglia, where the activity of single neurons was recorded. Currently,

(E–G) Dose responses of L4 DRG neuron activation in response to mechanical press (from mild 50 g to noxious 500 g) using naive or CFA-treated *Pirt-GCaMP6* mice (n = 3 per group). The percentage of coupled activated neurons in (E) was calculated from the number of coupled activated neurons divided by the number of total activated neurons (F for naive mice, G for CFA-treated mice).

(H and I) Examining neuronal coupling in response to noxious heat (48°C) in naive and CFA-treated *Pirt-GCaMP3* mice. There are significant increases in the numbers of total activated neurons and coupled activated neurons (H) and the percentage of coupled activated neurons in CFA-treated mice compared to naive mice (I; n = 3; p < 0.05). The data are presented as mean ± SEM.

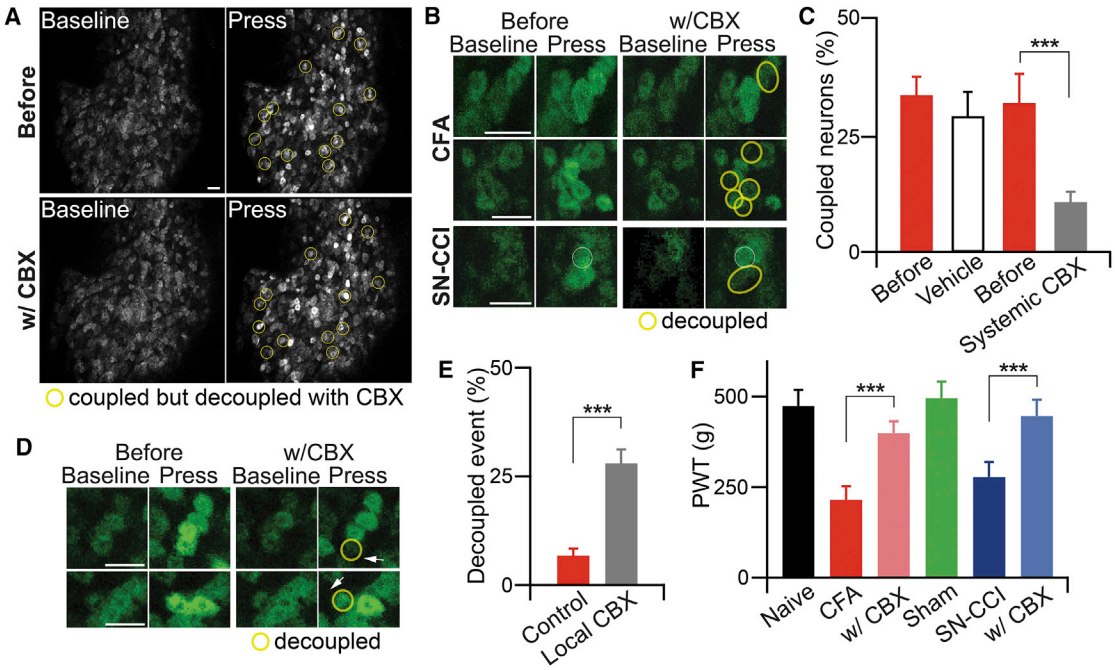

Figure 5. Coupling Event and Pain Hypersensitivity Are Significantly Attenuated by the Gap Junction Blocker Carbenoxolone

(A) Representative images of coupled and decoupled events before and approximately 1 hr after systemic gap junction blocker carbenoxolone (CBX) injection (100 mg/kg, i.p.) in in vivo calcium imaging of whole L4 DRG neurons. Yellow circles indicate coupled events in which adjacent DRG neurons tend to activate together and these coupled events decoupled by systemic CBX. Scale bar, 50 μm.

(B) Example images of coupled and decoupled events by systemic application of CBX. Yellow circles indicate the coupled DRG neurons decoupled by systemic CBX. Scale bar, 50 μm.

(C) Percentage change of coupled DRG neurons out of total activated DRG neurons by vehicle or CBX.

(D) Decoupled images of coupled events by local CBX injection using glass pipette electrode into DRG tissue. Yellow circles indicate decoupled DRG neurons. Arrows indicate where CBX was injected into the DRG tissue. Scale bar, 50 μm.

(E) Quantification of decoupled events in control coupled events and coupled events after local CBX injection into DRG tissue.

(F) PWT was tested at the hindpaw of naive, CFA, CFA with CBX, sham, SN-CCI, and SN-CCI with CBX animals by rodent pincher. The data are presented as mean ± SEM. ***$p < 0.001$.

recording of single DRG neurons in live animals can only be achieved in few laboratories (Ma et al., 2010). The new in vivo DRG imaging method using the genetically encoded Ca^{2+} indicator GCaMP that we have developed allowed us to observe cellular interactions under conditions that are close to physiological and enabled the correlation between coupled activation of neurons and pain behavior. Neuronal coupling represents a novel form of neuronal plasticity that is difficult to detect by conventional single-neuron recordings. Therefore, in vivo DRG imaging will open new avenues to study the role of primary sensory neurons in different somatosensations, including pain, itch, and touch.

Neuronal "cross talk" has been first described by Devor and Wall (1990) and was proposed to be mediated chemically (Amir and Devor, 1996). Here our dual patch recordings provided direct evidence for both neuron-SGC and neuron-neuron electrical coupling. To our best knowledge, this is the first direct demonstration of such coupling. We also show that DRG neurons communicate, at least in part, by gap junctions. However, our results do not exclude chemical communications as proposed by previous studies. The patch-clamp recordings, dye coupling, and Cx43CKO results suggest that SGCs participate in coupled activation. Indeed, the major mechanism by which astrocytes communicate is by calcium waves, which are mediated via both gap junctions and chemical messengers (Scemes and Giaume, 2006). This also appears to hold for sensory ganglia, where both neurons and SGCs participate in these waves (Suadicani et al., 2010). The pathway connecting the neurons is not clear, but transmission from neuron to SGC to neuron is feasible, with neurons and SGCs forming heterotypic gap junctions (i.e., Cx43 hemichannels in glia connect with other connexin hemichannels in neurons) (Damodaram et al., 2009; Thalakoti et al., 2007). A scheme where SGCs intervene chemically between neurons has been proposed (Rozanski et al., 2013). Both our imaging (Figures 4H and 4I) and behavioral data (Figure S1) suggest that neuronal coupling induced by tissue injury contributes more to mechanical hyperalgesia and allodynia than heat hyperalgesia, which requires further investigation. Coupled neuronal activation represents a novel mechanism underlying mechanical hyperalgesia (stronger pain by recruiting more nociceptors) and allodynia (non-painful LTMRs recruiting nociceptors). Therefore, inhibiting gap-junction-mediated coupling may provide a novel way to relieve mechanical hyperalgesia and allodynia.

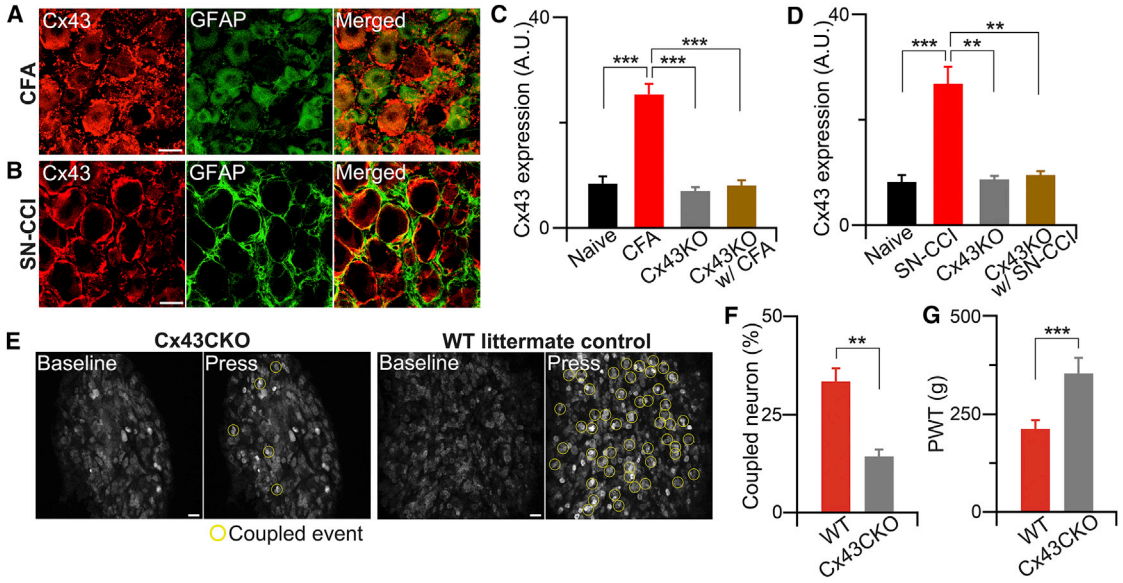

Figure 6. Gap Junction Protein Cx43 Promotes Coupling Event and Contributes to Pain

(A) Representative confocal images of Cx43 and GFAP staining from DRG of WT littermate control animals after inflammation. DRG from mice 2 days after CFA injection were stained with anti-GFAP (for SGCs; green) and/or anti-Cx43 (red) antibodies. Scale bar, 20 μm.

(B) Representative confocal Cx43 and GFAP staining images from DRG of WT littermate control animals after nerve injury. DRG slices from mice 7 days after nerve injury were stained with anti-GFAP (green) and/or anti-Cx43 (red) antibodies. Scale bar, 20 μm.

(C and D) Percentage change of Cx43 levels in DRG from naive and CFA- (C) or SN-CCI- (D) treated WT animals and also from conditional *Cx43CKO* animals. Data are expressed as the mean density. Cx43 level from WT DRG (n = 10, 8.44 ± 1.38 a.u.), CFA DRG (n = 10, 25.42 ± 1.99), CCI DRG (n = 8, 26.83 ± 3.30), and *Cx43CKO* DRG (n = 10, 7.04 ± 0.68).

(E) Representative in vivo confocal images of whole L4 DRG neurons from *Cx43CKO* and WT littermate control animals after CFA. Yellow circles indicate coupled event.

(F) Percentage change of coupled DRG neurons from *Cx43CKO* and WT littermate control animals (i.e., *Cx43 flox* allele without *PLP-Cre* mice).

(G) PWT was tested in *Cx43CKO* and WT littermate control animals with rodent pincher. The data are expressed as PWT values and presented as mean ± SEM. $^{**}p < 0.01$, $^{***}p < 0.001$.

EXPERIMENTAL PROCEDURES

Animals

Pirt-GCaMP3 mice were generated and described in a previous study (Kim et al., 2014). Briefly, the animal is generated by targeted homologous recombination to replace the entire coding region of the *Pirt* gene with the *GCaMP3* sequence and put in frame with the Pirt promoter. *GCaMP3* cDNA was provided by the laboratory of Loren Looger (Janelia Research Campus). Conditional Cx43KO mice were made by crossing between *loxp-ROSA-Cx43* mice and *PLP-CreER* mice, which were obtained from The Jackson Laboratory. *Npy2r* mice were obtained from Gensat. *Pirt-GCaMP6s* mice were generated by crossing *Pirt-Cre* with *Rosa26-LoxP-STOP-LoxP-GCaMP6s* mice. *Pirt-GCaMP3* and *Pirt-GCaMP6s* heterozygotes were used in all animal experiments otherwise indicated.

Animal Models

All experiments were performed in accordance with a protocol approved by the Animal Care and Use Committee at the Johns Hopkins University School of Medicine. Animals were group housed, unless otherwise mentioned, at 23°C with ad libitum access to food and water in a regular light/dark cycle. The mice used in the tests were backcrossed to C57Bl/6 mice for at least ten generations and were 3 to 4 months old (20–30 g) from both sexes. To generate the CFA inflammatory model, we mixed CFA and saline with a 1:1 ratio and injected them (10 μL) subcutaneously into glabrous skin of the hindpaw. Two days later, imaging experiments and/or behavioral experiments and immunohistochemistry were performed.

To generate the SN-CCI nerve injury model, we anesthetized mice with sodium pentobarbital (40–50 mg/kg, i.p.). SN was exposed at the level of the mid-thigh by a small dissection, and the nerve was isolated from surrounding tissues. The chronic constriction injury was performed by wrapping loose nylon ligatures around the unilateral SN. The incision was closed with sutures or tissue glue. Sham-operated mice received only an identical dissection of the unilateral nerve exposure and nerve isolation without the ligature. Seven to ten days after the SN-CCI surgery, imaging and behavioral experiments and immunohistochemistry were performed.

Tamoxifen Injection

10 mg of tamoxifen (Sigma) were dissolved in 1 mL of 100% sunflower oil and made fresh before use. *Cx43* WT and *Cx43CKO* mice both received tamoxifen injection (by gavage) at 100 mg/kg once before (usually 7 days before) the experiment was performed. *Cx43CKO* refers to mice that received tamoxifen injection. Behavioral assays were performed on mice after 7 days of tamoxifen injection. *Cx43CKO* mice were healthy, and there was no visible difference compared to Cx43 WT littermate control mice, in which only *PLP-CreER* gene was missing.

Behavioral Tests

Behavioral tests were conducted by experimenters blind to conditions. To test PWT, they placed mice in a 2.5-cm-diameter tube and habituated them to the tube in a behavioral room for at least 30 min per day for 3 days prior to any testing procedures. The hindpaws were outside the tube, enabling mechanical stimulation. Rodent pincher analgesia meter (IITC Life Science, CN, product #2450) was pressed to the hindpaws, and an active withdrawal of the stimulated hindpaw or any vocalization during the press was defined as a response. The pincher meter was applied ten times at intervals of at least 30 s.

Hot Plate Methods

Mice were placed in a clear plexiglass cylinder on top of a temperature-controlled metal plate (Life Science Series 8, Model 39.) The latency of acute nocifensive responses was determined by the onset of hindpaw lifts and/or licking, flinching, or jumping.

Tail Immersion Test

Mice were restrained in an apparatus made of 50 mL conical tubes. Their tails were exposed in the water bath set to the designated temperatures.

Von Frey Methods

Mice were placed in a transparent plastic box (4.5 × 5 × 10 cm) on a metal mesh and acclimatized for 30 min prior to testing. Each mouse was tested more than five times at a specific force manually, and the threshold was determined by the lowest force needed to elicit responses more than 50% of the time.

Hargreaves Test

Mice were placed under a transparent plastic box (4.5 × 5 × 10 cm) on a glass platform (Plantar Test Apparatus, IITC Life Science). Radiant heat was adjusted to 18% of maximal output and shone on the center of the paws. Each mouse was tested more than three times, with each test performed 20 min apart.

DRG Exposure Surgery for In Vivo Imaging of the Whole L4 DRG

For all imaging experiments, mice 3 months or older were anesthetized by i.p. injection of sodium pentobarbital (40–50 mg/kg). After deep anesthesia was reached, the animal's back was shaved and aseptically prepared, and ophthalmic ointment (Lacrilube; Allergen Pharmaceuticals) was applied to the eyes to prevent drying. During the surgery, mice were kept on a heating pad (DC temperature controller, FHC) to maintain body temperature at 37°C ± 0.5°C as monitored by a rectal probe.

Dorsal laminectomy in DRG was performed usually at spinal level L6 to S1 below the lumbar enlargement (but occasionally at lower than S1) but without removing the dura (some experimental conditions, such as direct local drug injection into DRG tissue and rhodamine injection into DRG neurons, required the removal of the dura). A 2-cm-long midline incision was made around the lower part of the lumbar enlargement area; next, 0.1 mL of 1% lidocaine was injected into the paravertebral muscles, and these were dissected away to expose the lower lumbar part which surrounds (L3–L5) vertebra bones. The L4 DRG transverse processes were exposed and cleaned. Using small rongeurs, we removed the surface aspect of the L4 DRG transverse process near the vertebra (only the L4 DRG transverse process was removed, but the bone over the spinal cord was intact) to expose the underlying DRG without damaging the DRG and spinal cord. Bleeding from the bone was stopped using styptic cotton.

In Vivo DRG Calcium Imaging

In vivo imaging of whole L4 DRG in live mice was performed for 1–6 hr immediately after the surgery. Body temperature was maintained at 37°C ± 0.5°C on a heating pad and rectal temperature was monitored. After surgery, mice were laid down in the abdomen-down position on a custom-designed microscope stage. The spinal column was stabilized using custom-designed clamps to minimize movements caused by breathing and heart beats. In addition, a custom-designed head holder was also used as an anesthesia/gas mask. The animals were maintained under continuous anesthesia for the duration of the imaging experiment with 1%–2% isoflurane gas using a gas vaporizer. Pure oxygen air was used to deliver the gas to the animal.

The microscope stage was fixed under a laser-scanning confocal microscope (Leica LSI microscope system), which was equipped with macro-based, large-objective, and fast EM-CCD camera. Live images were acquired at typically eight to ten frames with 600 Hz in frame-scan mode per 6–7 s, at depths below the dura ranging from 0 to 70 μm, using a 5× 0.5 NA macro dry objective at typically 512 × 512 pixel resolution with solid diode lasers (Leica) tuned at 488 and at 532 nm wavelength and emission at 500–550 nm for green and 550–650 nm for red fluorescence, respectively. For analysis, raw image stacks (512 × 512 to 1024 × 1024 pixels in the x–y plane and 20–30 μm voxel depth; typically 10 optical sections) were imported into ImageJ (NIH) for further analysis. DRG neurons were at the focal plane, and imaging was monitored during the activation of DRG neuron cell bodies by peripheral stimuli. Red fluorescent signal was used to identify Npy2r cell type, DiI tracing, and rhodamine transfer. The imaging parameters were chosen to allow repeated imaging of the same cell over many stimuli without causing damage to the imaged cells or to surrounding tissue.

Stimulus Delivery during Imaging Experiments

Press stimuli were delivered using rodent pincher analgesia meter, which was pressed to the hindpaws of mice. The press force was controlled manually by the experimenter. The duration of the press is 15–30 s after 40–50 s of baseline imaging.

In Vivo Calcium Imaging Data Analysis

For imaging data analysis, raw image stacks were collected, deconvoluted (if needed), and imported into ImageJ (NIH) for further analysis. Optical planes from sequential time points were first re-aligned and motion corrected using a cross-correlation-based image alignment plugin in ImageJ software to compensate for minor motion change during the acquisition. The contrast was adjusted, and selected optical planes or z projections of sequential optical sections were used to obtain final images and to produce time-lapse movies.

Calcium signal amplitudes were expressed as $(F_t - F_0)/F_0$ as a function of time, ratio of fluorescence difference $(F_t - F_0)$ to basal value (F_0). The average fluorescence intensity in the baseline period was taken as F_0 and measured as the average pixel intensity during the first two to six frames of each imaging experiment. The maximum fluorescence intensity F_t was measured by calculating the average (peak – background) pixel values in a given region of interest (ROI) for each image frame recorded during a time interval before and during the stimulation period. The F_t was then used to calculate ΔF/F using the formula $\Delta F/F = (F_t - F_0)/F_0$.

All putative responding cells were verified by visual examination using the raw imaging data. First, analyzers visually scored cells to identify press-evoked calcium transients in DRG neurons by directly observing the aligned image data displayed as a relative fluorescence movie, as well as the putative responding cells' fluorescence time series. Analyzers defined calcium transients as press evoked if their onsets occurred between the start of press stimulus and the 7 s after the end of the stimulus (it takes about 6–7 s to obtain a full, single DRG image). For zoomed-in faster scanning, it takes 0.47 s/frame to image individual ensembles of coupled neurons. Neuronal coupling was defined as two or more neuronal cell bodies located within 1 μm of each other showing increases in GCaMP signals between two imaging frames. The average ΔF/F values for specific ROIs were tested for statistical significance by repeated-measures ANOVA, followed by Mann-Whitney statistics. ImageJ or Fiji (NIH) and LIF (Leica) software were used to analyze Ca^{2+} imaging data using standard functions and a custom macro.

Systemic and Local CBX Injection and Rhodamine Injection

CBX (Sigma) was dissolved in saline. Animals received systemic CBX by i.p. injection. CBX (50 μM in saline) was injected into the DRG from a micropipette by pressure. After the injection, the micropipette was left in the tissue for 4–5 min, and then it was withdrawn. Rhodamine (Life Technologies) was injected from a micropipette into DRG neurons.

Immunohistochemistry

Adult Cx43 WT control littermate and Cx43CKO animals (12–20 weeks old) with different conditions (naive, 2 days after CFA, and 7 days after nerve injury) were deeply anesthetized with 3% isoflurane and transcardially perfused with 50 mL 0.1 M cold PBS followed by 50 mL PBS containing 4% paraformaldehyde (PFA) (pH 7.4; 4°C). DRGs and lumbar enlargement of the spinal cord were dissected from the perfused mice, postfixed in 4% PFA at 4°C overnight, cryoprotected in 30% sucrose in PBS at 4°C overnight, and frozen in cryo-embedding media (OCT) at −80°C using dry ice. Tissues were transversely sectioned (20 μm) with a cryostat. The sections collected on slides were dried at 37°C for 20 min, then washed with PBS containing 0.2% Triton X-100 (PBT) and blocked with 10% goat or donkey serum in PBT for 1 hr. All sections were simultaneously incubated overnight with primary antibodies diluted in blocking solution at 4°C. Primary antibodies were rabbit anti-Cx43 (C6219; Sigma; 1:3,000), mouse anti-GFAP (glial fibrillary acidic protein) (CN, MAB360; Millipore; 1:700), rat anti-CGRP (CN, 1720-9007; AbD Serotec; 1:1,000), and

fluorescein-labeled *Griffonia simplicifolia* lectin (GSL) I-isolectin B_4 (CN, FL-1201; Vector Laboratories; 1:1,000). After incubation with primary antibody, sections were washed with PBT and then incubated for 2 hr at room temperature in solutions containing species-specific secondary antibodies conjugated to Alexa 488 or 568 (Molecular Probes). The secondary antibodies were diluted 1:1,000 in blocking solution. Following washes with PBS, the stained sections were mounted and coverslipped with Vectashield (Vector Laboratories). The sections were examined and immunostaining images were obtained with a Zeiss 700 scanning confocal microscope.

DiI Labeling and Imaging

To determine how well the in vivo imaging represents the whole population of the DRG neurons, we injected the retrograde nerve tracer DiI (Life Technologies, 0.1% in methanol) into the hindpaws and observed it in neuronal cell bodies in the DRG.

DRG Cultures

C57BL/6 mice of either sex (2–3 months old; Charles River or The Jackson Laboratory) were anesthetized with isoflurane (Abbott Laboratories) and euthanized by decapitation. The DRG were removed as described (Huang et al., 2005) and transferred into cold Dulbecco's PBS (DPBS [pH 7.4]; Mediatech Cellgro). Next, they were cleaned from connective tissue and transferred to 1.5 mL vials containing DPBS and collagenase (1 mg/mL, Type 1A; Sigma). The vial was then placed on a tilting stage (with a rate of 50 min^{-1}) for 45 min at 37°C. After this digestion period, the collagenase solution was substituted by fresh DPBS; the ganglia were then triturated by repeated pipetting until tissue dissociation, spun down (1,000 rpm for 5 min), re-suspended, placed in glass-bottomed MatTek dishes (MatTek) in DMEM (GIBCO, Invitrogen) supplemented with 10% fetal bovine serum (GIBCO) and 1% penicillin-streptomycin (Mediatech Cellgro), and transferred to a humidified 5% CO_2 incubator at 37°C. Cultures were generally used at 3–18 hr (for acute culture) or 1–2 days after their preparation when the cultures typically consisted of neurons closely apposed by SGCs, whose identity could be confirmed by their positive immunoreactivity for the marker glutamine synthetase, shape, size, and absence of inward currents upon depolarization. Viability of neurons in the cultures was confirmed by their ability to fire action potentials and inducibility of inward currents.

Electrophysiology

Neuron-SGC and neuron-neuron pairs were used for dual whole-cell patch-clamp recordings performed at room temperature on cells bathed in solution containing 140 mM NaCl, 2 mM $CsCl_2$, 1 mM $MgCl_2$, 5 mM HEPES, 2 mM KCl, 5 mM glucose, 2 mM sodium pyruvate, and 1 mM $BaCl_2$. Patch pipettes (4–6 MΩ) were filled with solution containing 130 mM CsCl (voltage clamp) or 130 mM KCl (current clamp), 10 mM EGTA, 10 mM HEPES, and 2 mM $CaCl_2$ and connected to an Axopatch 1D amplifier (Molecular Devices). Data were acquired with Clampex 6.0 or 8.2 software, digitized using an Axon Instruments Digitizer, and analyzed with Clampfit 9.0 or later software (Molecular Devices). Cells were generally held at −60 mV unless otherwise indicated. Junctional conductance (gj) was calculated as the current recorded in one cell in response to voltage ramps or steps applied to the other cell of the pair (gj = i2/−v1) (del Corsso et al., 2006).

Dye Coupling in Intact Ganglia

After their removal from the animals, DRG were attached to a Sylgard (Dow Corning)-covered dish filled with cold Krebs solution. The connective tissue capsule around the ganglia was removed by fine dissection. No enzymes were used. The dishes were placed on the stage of an upright microscope (Zeiss) equipped with fluorescent illumination and a digital camera. The experiments were started about 30 min after removal. The dish was superfused with Krebs solution, which contained: 118 mmol/L NaCl, 4.7 mmol/L KCl, 14.4 mmol/L $NaHCO_3$, 1.2 mmol/L $MgSO_4$, 1.2 mmol/L NaH_2PO_4, 2.5 mmol/L $CaCl_2$, and 11.5 mmol/L glucose (pH 7.3). This solution was bubbled with a mixture of 95% O_2/5% CO_2. Individual cells in DRG were injected with the fluorescent dye lucifer yellow (LY; Sigma), 3% in 0.5 mol/L LiCl solution from sharp glass microelectrodes connected to an electrometer (Neuro Data Instruments Corp.) (Huang et al., 2005). The dye was passed by hyperpolarizing current pulses, 100 ms in duration, with 0.5–1 nA in amplitude at 5 Hz for about 2 min. The injections were made under visual inspection to allow cell identification. At the end of the injection of each cell, we counted the number of cells that were labeled as a result of dye passage from the injected cell (dye-coupled cells). After the experiments, the DRG were fixed for 20 hr at 4°C in 4% PFA in PBS (pH 7.4), washed with PBS, and mounted in gel/mount (Biomeda). The LY-labeled cells were imaged with a confocal microscope (Bio-Rad).

Analysis

Group data were expressed as mean ± SEM. Unless otherwise noted, two-tailed unpaired Student's t test and/or Mann-Whitney statistical test were used to determine significance in statistical comparisons, and differences were considered significant at $p < 0.05$. Animal behavior data were analyzed with two-way ANOVA test.

SUPPLEMENTAL INFORMATION

Supplemental Information includes two figures and six movies and can be found with this article online at http://dx.doi.org/10.1016/j.neuron.2016.07.044.

AUTHOR CONTRIBUTIONS

Y.S.K. conceived the project, designed and performed most imaging and behavioral experiments, and wrote and edited the paper. Y.S.K., M.A., and K.P. analyzed the data. K.P., M.A., and Q.Z. performed in vivo DRG surgery and imaging and behavioral experiments. S. performed in vivo DRG surgery with supervision from F.Z. C.G. and S.H. performed immunohistochemistry with supervision from Y.G. C.G. and L.Y. counted cell size and number. Y.S.K., K.P., C.G., and L.Y. maintained, set up mating, took care of mice, and performed genotyping. D.C.S. performed the patch-clamp recordings. A.A. and D.B. generated *Rosa26-LSL-GCaMP6s* mice. P.C.L. and M.H. wrote and edited the paper. X.D. supervised the project and wrote and edited the paper.

ACKNOWLEDGMENTS

We thank members of X.D. laboratories for helpful comments and discussion. We also thank JHU pain research imaging core for its assistance. This work was supported by National Institutes of Health Grants (R01DE022750 and R01GM087369 to X.D.), Johns Hopkins University Brain Science Institute grant, and HHMI. M.H. was supported by ISF (508/13) and BSF (201144).

Received: January 19, 2016
Revised: June 21, 2016
Accepted: July 19, 2016
Published: August 25, 2016

REFERENCES

Amir, R., and Devor, M. (1996). Chemically mediated cross-excitation in rat dorsal root ganglia. J. Neurosci. *16*, 4733–4741.

Basbaum, A.I., and Woolf, C.J. (1999). Pain. Curr. Biol. *9*, R429–R431.

Basbaum, A.I., Bautista, D.M., Scherrer, G., and Julius, D. (2009). Cellular and molecular mechanisms of pain. Cell *139*, 267–284.

Belzer, V., Shraer, N., and Hanani, M. (2010). Phenotypic changes in satellite glial cells in cultured trigeminal ganglia. Neuron Glia Biol. *6*, 237–243.

Blum, E., Procacci, P., Conte, V., and Hanani, M. (2014). Systemic inflammation alters satellite glial cell function and structure. A possible contribution to pain. Neuroscience *274*, 209–217.

Damodaram, S., Thalakoti, S., Freeman, S.E., Garrett, F.G., and Durham, P.L. (2009). Tonabersat inhibits trigeminal ganglion neuronal-satellite glial cell signaling. Headache *49*, 5–20.

del Corsso, C., Srinivas, M., Urban-Maldonado, M., Moreno, A.P., Fort, A.G., Fishman, G.I., and Spray, D.C. (2006). Transfection of mammalian cells with

connexins and measurement of voltage sensitivity of their gap junctions. Nat. Protoc. *1*, 1799–1809.

Devor, M., and Wall, P.D. (1990). Cross-excitation in dorsal root ganglia of nerve-injured and intact rats. J. Neurophysiol. *64*, 1733–1746.

Doerflinger, N.H., Macklin, W.B., and Popko, B. (2003). Inducible site-specific recombination in myelinating cells. Genesis *35*, 63–72.

Dublin, P., and Hanani, M. (2007). Satellite glial cells in sensory ganglia: their possible contribution to inflammatory pain. Brain Behav. Immun. *21*, 592–598.

Garrett, F.G., and Durham, P.L. (2008). Differential expression of connexins in trigeminal ganglion neurons and satellite glial cells in response to chronic or acute joint inflammation. Neuron Glia Biol. *4*, 295–306.

Hanani, M. (2005). Satellite glial cells in sensory ganglia: from form to function. Brain Res. Brain Res. Rev. *48*, 457–476.

Hanani, M. (2012). Intercellular communication in sensory ganglia by purinergic receptors and gap junctions: implications for chronic pain. Brain Res. *1487*, 183–191.

Huang, T.Y., Cherkas, P.S., Rosenthal, D.W., and Hanani, M. (2005). Dye coupling among satellite glial cells in mammalian dorsal root ganglia. Brain Res. *1036*, 42–49.

Huang, T.Y., Belzer, V., and Hanani, M. (2010). Gap junctions in dorsal root ganglia: possible contribution to visceral pain. Eur. J. Pain *14*, 49.e1–49.e11.

Huang, L.Y., Gu, Y., and Chen, Y. (2013). Communication between neuronal somata and satellite glial cells in sensory ganglia. Glia *61*, 1571–1581.

Kim, Y.S., Chu, Y., Han, L., Li, M., Li, Z., Lavinka, P.C., Sun, S., Tang, Z., Park, K., Caterina, M.J., et al. (2014). Central terminal sensitization of TRPV1 by descending serotonergic facilitation modulates chronic pain. Neuron *81*, 873–887.

Li, L., Rutlin, M., Abraira, V.E., Cassidy, C., Kus, L., Gong, S., Jankowski, M.P., Luo, W., Heintz, N., Koerber, H.R., et al. (2011). The functional organization of cutaneous low-threshold mechanosensory neurons. Cell *147*, 1615–1627.

Liu, Y., and Ma, Q. (2011). Generation of somatic sensory neuron diversity and implications on sensory coding. Curr. Opin. Neurobiol. *21*, 52–60.

Ma, C., Donnelly, D.F., and LaMotte, R.H. (2010). In vivo visualization and functional characterization of primary somatic neurons. J. Neurosci. Methods *191*, 60–65.

Ohara, P.T., Vit, J.P., Bhargava, A., and Jasmin, L. (2008). Evidence for a role of connexin 43 in trigeminal pain using RNA interference in vivo. J. Neurophysiol. *100*, 3064–3073.

Pannese, E. (2010). The structure of the perineuronal sheath of satellite glial cells (SGCs) in sensory ganglia. Neuron Glia Biol. *6*, 3–10.

Rozanski, G.M., Nath, A.R., Adams, M.E., and Stanley, E.F. (2013). Low voltage-activated calcium channels gate transmitter release at the dorsal root ganglion sandwich synapse. J. Physiol. *591*, 5575–5583.

Scemes, E., and Giaume, C. (2006). Astrocyte calcium waves: what they are and what they do. Glia *54*, 716–725.

Schmalbruch, H. (1987). The number of neurons in dorsal root ganglia L4-L6 of the rat. Anat. Rec. *219*, 315–322.

Sørensen, B., Tandrup, T., Koltzenburg, M., and Jakobsen, J. (2003). No further loss of dorsal root ganglion cells after axotomy in p75 neurotrophin receptor knockout mice. J. Comp. Neurol. *459*, 242–250.

Suadicani, S.O., Cherkas, P.S., Zuckerman, J., Smith, D.N., Spray, D.C., and Hanani, M. (2010). Bidirectional calcium signaling between satellite glial cells and neurons in cultured mouse trigeminal ganglia. Neuron Glia Biol. *6*, 43–51.

Thalakoti, S., Patil, V.V., Damodaram, S., Vause, C.V., Langford, L.E., Freeman, S.E., and Durham, P.L. (2007). Neuron-glia signaling in trigeminal ganglion: implications for migraine pathology. Headache *47*, 1008–1023, discussion 24–25.

Zhang, H., Mei, X., Zhang, P., Ma, C., White, F.A., Donnelly, D.F., and Lamotte, R.H. (2009). Altered functional properties of satellite glial cells in compressed spinal ganglia. Glia *57*, 1588–1599.

Zuriel, E., and Devor, M. (2001). Dye coupling does not explain functional crosstalk within dorsal root ganglia. J. Peripher. Nerv. Syst. *6*, 227–231.